LETTER
SPACE PHYSICS: MAGNETOSPHERIC PHYSICS

Earth and Planetary Physics
10: 524–533, 2026
doi: 10.26464/epp2026042

Characteristics of energy conversion and energy flux densities at the Kelvin–Helmholtz vortex

ZhiZhong Guo[1,2], Zhe Wang[1,2*], HuiShan Fu[1,2*], WenZhe Zhang[1,2], ChenXi Du[1,2], WenDing Fu[1,2], ZhenYu Xu[1,2], and JiQiu Niu[1,2]

[1]School of Space and Earth Sciences, Beihang University, Beijing 102206, China;

[2]Key Laboratory of Space Environment Monitoring and Information Processing, Ministry of Industry and Information Technology, Beijing 102206, China

Key Points:

- The linear Kelvin–Helmholtz (KH) vortex can be a generator region ($\int \boldsymbol{J}\cdot\boldsymbol{E} < 0$), whereas the nonlinear KH vortex can be a load region ($\int \boldsymbol{J}\cdot\boldsymbol{E} > 0$).
- At the linear KH vortex, ion enthalpy, ion heat, and Poynting fluxes collaboratively contribute to the energy transfer.
- At the nonlinear KH vortex, Poynting fluxes carry the greatest energy and ions play a less important role in energy transfer.

Citation: Guo, Z. Z., Wang, Z., Fu, H. S., Zhang, W. Z., Du, C. X., Fu, W. D., Xu, Z. Y., and Niu, J. Q. (2026). Characteristics of energy conversion and energy flux densities at the Kelvin–Helmholtz vortex. *Earth Planet. Phys.*, *10*(3), 524–533. http://doi.org/10.26464/epp2026042

Abstract: The Kelvin–Helmholtz (KH) instability serves as an important process for transporting the solar wind mass and energy into the Earth's magnetosphere. However, energy conversion and energy transport at the vortices driven by the KH instability have not been investigated in detail thus far. Here, using high-resolution data from the Magnetospheric Multiscale (MMS) spacecraft, we compare characteristics of energy conversion and energy flux densities between a linear and a nonlinear KH vortex. We find that the linear KH vortex is acting as a generator region ($\int \boldsymbol{J}\cdot\boldsymbol{E} < 0$, where $\boldsymbol{J}$ is the current density and $\boldsymbol{E}$ is the electric field) whereas the nonlinear KH vortex is a load region ($\int \boldsymbol{J}\cdot\boldsymbol{E} > 0$). The energy flux densities increase significantly at the trailing edge of KH vortices. At the linear KH vortex, energy transfer is equally contributed by enthalpy, ion kinetic, and Poynting fluxes, whereas in the nonlinear case, the energy is mainly transported in the form of the Poynting flux and electron kinetic energy and heat fluxes are negligible. These results help us better understand the role of KH vortices in energy conversion and transport at the Earth's magnetopause.

Keywords: magnetopause; Kelvin–Helmholtz instability; energy conversion

1. Introduction

The magnetopause is defined as the ion-scale boundary between the shocked solar wind and the magnetosphere (Le and Russell, 1994; De Keyser et al., 2005; Sun et al., 2024). It adjoins the magnetosheath boundary layer, the low-latitude boundary layer, the entry layer, the cusp, and the plasma mantle (Phan et al., 1997; Eastman et al., 2000; Lin RL et al., 2010; Yao ZH et al., 2024). The magnetopause prevents solar wind plasma from directly entering the magnetosphere and is of crucial importance for the mass, momentum, and energy transfer from the magnetosheath into the magnetosphere (Pu et al., 1983; Johnson and Cheng CZ, 1997; Hasegawa, 2012; Fu HS et al., 2019a, b). Previous theoretical and observational studies have indicated that the interplanetary magnetic field (IMF) and the solar wind plasma greatly influence the global dynamics of the magnetopause (Shue et al., 1998; Wang Z et al., 2020a; Fu WD et al., 2025a). During the southward IMF, reconnection between the magnetosheath magnetic field and the magnetospheric magnetic field is frequently observed at the dayside magnetopause (Burch et al., 2016a; Chen LJ et al., 2016; Cao D et al., 2017; Cassak et al., 2017; Wang Z et al., 2019; Huang SY et al., 2021, 2025; Liu YN et al., 2024). In contrast, the Kelvin–Helmholtz (KH) instability driven by the velocity shear between the plasma in the magnetosphere and that in the magnetosheath dominates the northward IMF scenario (Miura, 1984; Otto and Fairfield, 2000; Nykyri and Otto, 2001; Hasegawa et al., 2006). Because it can form a surface wave at the magnetopause, such an instability is also known as a "KH wave" (Rice et al., 2022; Radhakrishnan et al., 2024). These processes occur with energy conversion between the magnetic field and plasma, making the magnetopause a key region in the solar–terrestrial energy chain (Dunlop and Balogh, 2005; Dong XC et al., 2018).

Previous studies using a three-dimensional (3D) global magnetohydrodynamic (MHD) simulation have suggested that the energy conversion at the dayside magnetopause is typically dominated by energy loads ($\boldsymbol{J}\cdot\boldsymbol{E} > 0$), whereas it acts as generator ($\boldsymbol{J}\cdot\boldsymbol{E} < 0$) at the tail magnetopause (Palmroth et al., 2003, 2006). Theoretically, the electromagnetic energy (primarily magnetic field energy) can

First author: Z. Z. Guo, zhizhongguo55@buaa.edu.cn
Correspondence to: Z. Wang, zhewang@buaa.edu.cn
H. S. Fu, huishanf@gmail.com
Received 12 DEC 2025; Accepted 27 FEB 2026.
First Published online 21 MAR 2026.
©2026 by Earth and Planetary Physics.

be converted through several energy channels, which can be expressed by the equation

$$\frac{\partial U_B}{\partial t} = -\frac{\partial U_{i,e}}{\partial t} - \nabla \cdot (\boldsymbol{S} + \boldsymbol{H}_{i,e} + \boldsymbol{K}_{i,e} + \boldsymbol{q}_{i,e}),$$

where U_B, $U_{i,e}$, $\boldsymbol{S}$, $\boldsymbol{H}_{i,e}$, $\boldsymbol{K}_{i,e}$, and $\boldsymbol{q}_{i,e}$ denote the magnetic field energy, particle total energy, Poynting flux, particle enthalpy flux, kinetic energy flux, and heat flux, respectively, with the subscripts i, e denoting ion species and electron species (Yamada et al., 2010; Eastwood et al., 2013; Goldman et al., 2016). To date, the energy conversion and the corresponding energy partitioning have been investigated in detail during the dayside magnetopause reconnection (Eastwood et al., 2020; Dong XC et al., 2021; Genestreti et al., 2022). Using the high-resolution Magnetospheric Multiscale (MMS) measurements, Fargette et al. (2024) found that the energy flux partition changes at the electron diffusion region and is locally dominated by the electron enthalpy flux. On the basis of a two-dimensional (2D) particle-in-cell simulation, Chang C et al. (2023) suggested that the Poynting flux provides electromagnetic energy for energy conversion near the magnetosphere separatrix region.

Although these studies greatly improve our understanding of energy conversion and transport at the magnetopause during the dayside magnetopause reconnection, energy conversion at the magnetopause with KH waves remains poorly understood thus far because earlier studies have mainly focused on their wavelength, period, the IMF conditions (Cowee et al., 2009; Lin D et al., 2014; Rice et al., 2022; Settino et al., 2022), and the plasma transport attributable to the KH waves (Nykyri and Otto, 2001; Smets et al., 2002; Sorathia et al., 2019; Yan GQ et al., 2020; Nakamura et al., 2022; Radhakrishnan et al., 2024). Previous studies have suggested that the KH waves at the Earth's magnetopause can transfer a significant amount of energy into the magnetosphere (Pu and Kivelson, 1983; Kavosi and Raeder, 2015), but the energy partitions still remain an open question. Moreover, various types of flow structures can be formed during the triggering and evolution of KH waves, such as the shear flow structures (linear KH vortex) at the initial stage of KH waves (Chandrasekhar, 1961; Fairfield et al., 2000; Wang Z et al., 2020b) and the roll-up vortices (nonlinear KH vortex) formed in the nonlinear stage of KH waves (Foullon et al., 2008; Hwang et al., 2012; Li W et al., 2016; Nykyri et al., 2017, Fu WD et al., 2025b). Therefore, one may also be curious about whether the energy conversion and transport are similar or dissimilar at these flow structures.

Kelvin–Helmholtz waves have been widely observed by the state-of-the-art MMS mission (Burch et al., 2016b), and a database has been built that includes either the linear stage or nonlinear stage of KH wave observations (Rice et al., 2022; Radhakrishnan et al., 2024), providing an excellent opportunity to answer these questions. Here, we conduct a case study to investigate the energy conversion and energy flux densities at two KH vortices on the dayside magnetopause. Specifically, one is the linear KH vortex observed during the initial stage of the KH wave, and the other is the nonlinear stage of the KH wave, where the KH vortices are fully rolled up (Radhakrishnan et al., 2024). Our results emphasize the role of the KH vortex in transporting energy into the Earth's magnetosphere and its contribution to understanding how the electromagnetic energy is converted into plasma energy at the magnetopause when the IMF is northward and the dayside magnetopause reconnection does not play a key role.

2. Data and Method

In this study, the data we utilize are all from the MMS mission (Burch et al., 2016b). Specifically, the magnetic field data are from the Fluxgate Magnetometer (Russell et al., 2016), the electric field data are from the Electric Double Probe (Lindqvist et al., 2016) and the Axial Double Probe (Ergun et al., 2016), and the plasma moment data are from the Fast Plasma Investigation (FPI) instrument (Pollock et al., 2016). Two KH events, which Radhakrishnan et al. (2024) identified as a linear KH event and a nonlinear KH event, are investigated in detail. The linear KH instability (KHI) event was observed by the MMS on October 10, 2016, when the spacecraft was located at [4.28, 10.53, −0.45] Earth radii (R_E) in Geocentric Solar Ecliptic (GSE) coordinates, with a phase velocity of 82.77 km/s; the nonlinear KHI event was observed by the MMS on November 12, 2019, when the spacecraft was located at [6.73, 11.14, 6.51] R_E in GSE coordinates, with a phase velocity of 86.99 km/s. Both were observed at the dayside magnetopause and have similar phase velocities, allowing a detailed comparison between them.

A common approach (the "standard decomposition"), which treats the plasma populations as a single distribution (Yamada et al., 2010; Eastwood et al., 2013, 2020), is used to investigate the energy flux densities at the magnetopause with the linear and nonlinear KHI. Specifically, the kinetic energy flux density of species s is estimated with

$$\boldsymbol{K}_s = \frac{1}{2} n m_s v_s^2 \boldsymbol{v}_s,$$

where n is the plasma number density, m_s is the particle mass, and $\boldsymbol{v}_s$ is the bulk velocity. The enthalpy flux density of species is estimated with

$$\boldsymbol{H}_s = \frac{\boldsymbol{v}_s \mathrm{Tr}(\overleftrightarrow{\boldsymbol{P}}_s)}{2} + \boldsymbol{v}_s \cdot \overleftrightarrow{\boldsymbol{P}}_s,$$

where $\boldsymbol{v}_s$ is the bulk velocity and $\overleftrightarrow{\boldsymbol{P}}_s$ is the pressure tensor, and $\mathrm{Tr}(\overleftrightarrow{\boldsymbol{P}}_s)$ is the trace of the pressure tensor. The Poynting flux density is estimated with

$$\boldsymbol{S} = \frac{\boldsymbol{E} \times \boldsymbol{B}}{\mu_0},$$

where $\boldsymbol{E}$ is the electric field in the spacecraft frame and is averaged to the resolution of the magnetic field $\boldsymbol{B}$. Finally, the heat flux $\boldsymbol{q}_s$ is obtained directly from the FPI data (Pollock et al., 2016).

2. Observation

Figure 1 presents an overview of the two KH events, with the linear KH wave case shown on the left (Figures 1a–1k) and the nonlinear KH wave case presented on the right (Figures 1l–1v). Figures 1a–1d display the large-scale context of the linear KH wave as observed by the MMS1 from 14:45 to 15:10 universal time (UT) on October 10, 2016. One can see that the omnidirectional ion energy spectrogram in Figure 1a shows quasi-periodic varia-

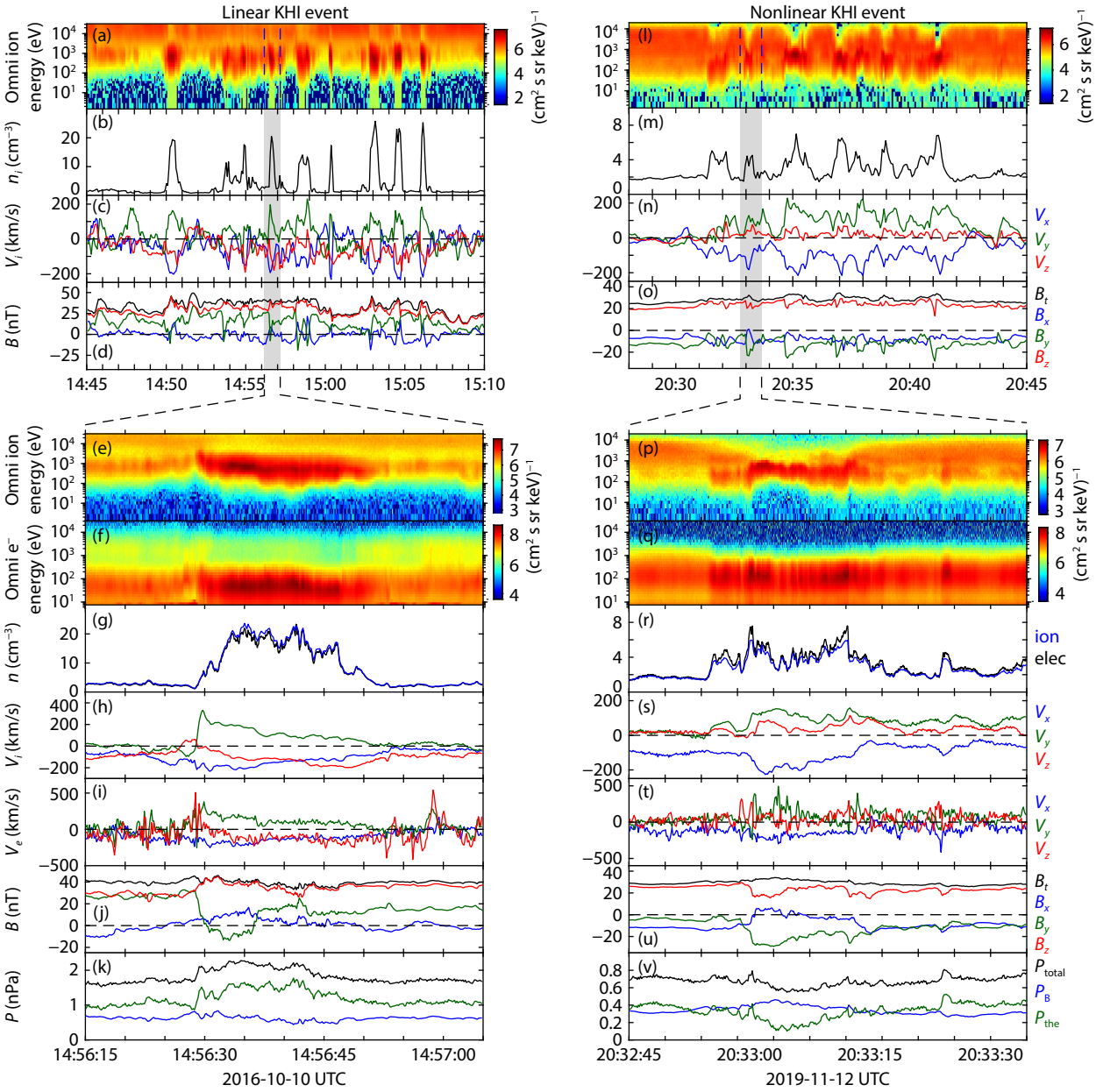

Figure 1. Observations of the linear KHI event (left) and the nonlinear KHI event (right), with (a–d, l–o) the large-scale context of the KHI interval and (e–k, p–v) detailed observations during the crossing of the KH vortex. Specifically, the (a, l) ion energy spectrum; (b, m) ion density; (c, n) ion velocity; (d, o) magnetic field; (e, p) ion energy spectrum; (f, q) electron energy spectrum; (g, r) ion and electron density; (h, s) ion velocity; (i, t) electron velocity; (j, u) magnetic field; and (e, p) pressure. All data are from the MMS1.

tions throughout the interval, which are well matched with the changes in the ion density (Figure 1b). Velocity shears on the order of 200 km/s occur regularly near the rapid changes in ion density (Figure 1c). The GSE magnetic field in Figure 1d shows fluctuations characteristic of a KH wave throughout the interval, with a magnitude of approximately 20 nT and bipolar variation in the normal component. All these features confirm it as a KH event. According to the periodic variations in density, ion velocity, and magnetic fields, one can see that 9 KH vortices are observed during this interval. Because the signatures of these vortices are very similar, we particularly focus on one KH vortex from 14:56:15 to 14:57:05 UT and show the data from this zoomed-in period in Figures 1e–1k. According to the omnidirectional ion energy spectrogram (Figure 1e), omnidirectional electron energy spectrogram (Figure 1f), and plasma density (Figure 1g), one can see that the MMS crossed the magnetopause from the magnetospheric side to the magnetosheath side at approximately 14:56:30 UT and vice versa at approximately 14:56:50 UT because of the existence of the KH wave. The low velocity of magnetospheric ions, the rapid change in magnetic field direction, and the increase in total pressure during the crossing indicate that it is a linear KH vortex that has not evolved to be fully rolled up (Rice et al., 2022; Radhakrishnan et al., 2024), as shown in the sketch in Figure 4a. The electron velocity is generally correlated to the ion velocity except for the

peaks on the magnetosphere side, indicating that the electrons are generally coupled with ions.

The nonlinear KH event, characterized by the existence of rolled-up vortices, was observed by the MMS from 20:28 to 20:45 UT on November 12, 2019. Figures 1l–1o show the large-scale context of the nonlinear KH wave as observed by the MMS1. Note that the nonlinear KH wave exhibits similar signatures as the linear KH wave, including the quasi-periodic fluctuations in omnidirectional ion spectra (Figure 1l), the corresponding variations in ion density (Figure 1m), the velocity shear on the order of 200 km/s (Figure 1n), the fluctuations around 8 nT in the total magnetic field, and the bipolar signatures in the magnetic field B_x, B_y components (Figure 1o). However, ions with magnetosphere-like density flowing with magnetosheath-like velocities are present (e.g., the velocity peaks before 20:34 UT and between 20:36 and 20:37 UT), suggesting that the vortices have developed. Similarly, one can identify 6 KH vortices in this interval according to the periodic variations of density and velocity. Because they have similar signatures, we selected one vortex from 20:32:45 to 20:33:40 UT as representative and show the detailed observations in Figures 1p–1v. We find that the plasma densities are less different on the magnetospheric side (approximately 2 cm^{-3}) and on the magnetosheath side (approximately 4 cm^{-3}), the velocity of magnetospheric ions is comparable to the velocity of magnetosheath ions, more small-scale structures appear on the electron velocity, quasi-periodic fluctuations with decreasing magnitude appear in the magnetic field, and a decrease in total pressure from 0.8 to 0.6 nPa appears. These features are indicative of the rolled-up vortices and suggest that it is a KH vortex at the nonlinear stage, as shown by the sketch in Figure 4b.

Theoretically, the energy conversion rate can be quantitatively estimated by the inner product of the current density and the electric field. Using this method, we investigate the energy conversion at the linear KH vortex and the nonlinear KH vortex; the result is shown in Figure 2. Figures 2a and 2g present the three components of the magnetic field in GSE coordinates, marking the crossing of the magnetopause. Figures 2b and 2h present the current density calculated by the curlometer technique. It has a higher time resolution than the current calculated with plasma moments. One can see that in the linear case, the current fluctuates greatly, with a higher magnitude on the magnetosheath side (approximately 400 nA/m^2) and a lower magnitude on the magnetospheric side (generally below 200 nA/m^2), whereas in the nonlinear case, an intense current (above 200 nA/m^2) appears only at the trailing edge of the KH wave, where the magnetic field direction changes significantly. Here, a trailing edge is represented by a crossing from the magnetosphere to the magnetosheath, and a reversed crossing indicates a leading edge (Li W et al., 2016). Figures 2c and 2i show the electric field measured by the MMS1. Note that in both cases, the electric field appears to be enhanced on the magnetosheath side, which is mainly due to the higher flow velocity there and thus the larger-scale convection electric field. Figures 2d–2e and 2j–2k show the energy conversion rate. As can be seen, the energy conversion rate peaks at the trailing edges of the KH vortices. Specifically, in the linear case, it can reach a negative value with a magnitude larger than −2 nW/m^3,

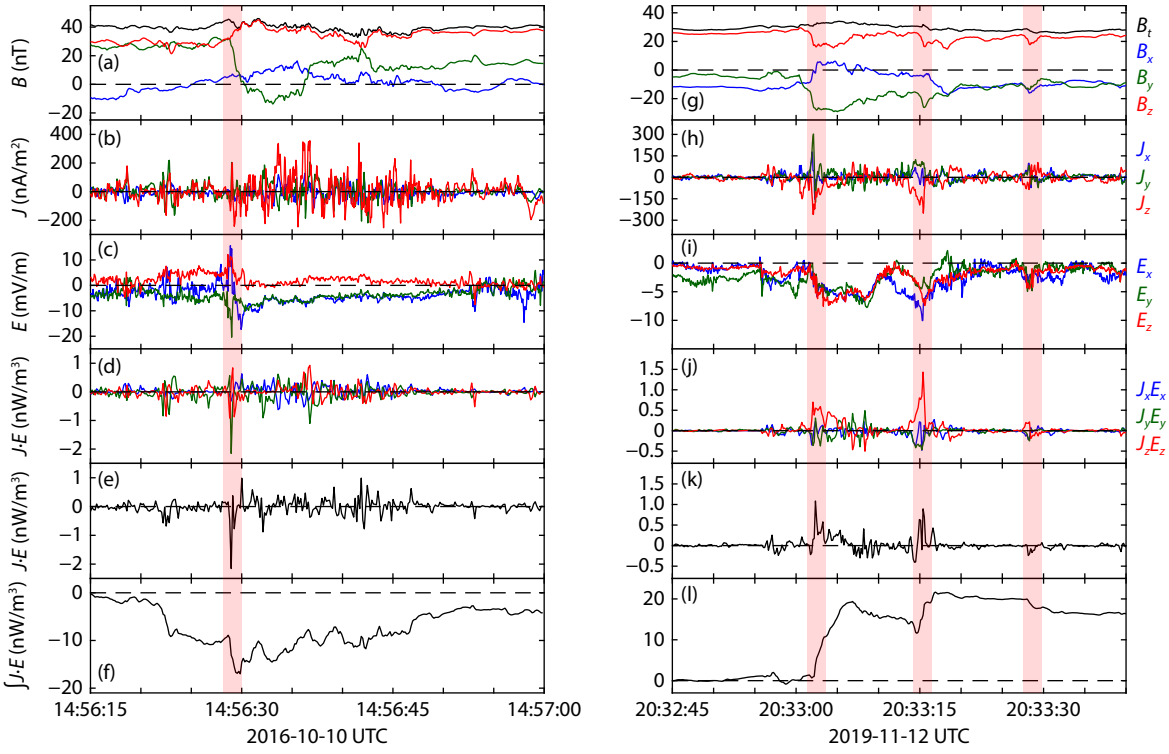

Figure 2. Strong energy conversion at the linear KH vortex (left) and nonlinear KH vortex (right). (a, g) Magnetic field; (b, h) current density estimated by the curlometer technique (Dunlop et al, 2002); (c, i) electric field; (d, j) energy conversion in different directions; (e, k) absolute value of the energy conversion; (f, l) accumulation of the energy conversion. The red shaded areas mark the trailing edge of the vortices.

whereas in the nonlinear case, it is generally positive, with the maximum value reaching approximately 1.2 nW/m^3. The strong energy conversion rate correlates well with the electric field, suggesting that the electric field being formed makes a significant contribution to the strong energy conversion. Moreover, the accumulation of the energy conversion rate shows a net negative value ($\int \boldsymbol{J}\cdot\boldsymbol{E} < 0$) throughout the interval in the linear KH vortex, with the peak value (−18 nW/m^3) at the trailing edge. Note also that the negative $\boldsymbol{J}\cdot\boldsymbol{E}$ occurs mainly on the magnetospheric side ahead of the trailing edge, whereas the positive $\boldsymbol{J}\cdot\boldsymbol{E}$ is dominant on the magnetosheath side, resulting in a decrease in the accumulation of net negative $\int \boldsymbol{J}\cdot\boldsymbol{E}$ (Figure 2f). On the contrary, the positive values of $\int \boldsymbol{J}\cdot\boldsymbol{E}$ dominate throughout the interval of the nonlinear KH vortex, with a rapid surge at the rolled-up trailing edges (a 20 nW/m^3 surge at the first encounter and a 10 nW/m^3 surge at the second encounter).

Figure 3 shows the energy flux densities at these two KH vortices. For the linear case, one can see that both the ion enthalpy flux (Figure 3c) and the ion kinetic energy flux (Figure 3d) rapidly increase across the trailing edge because of the presence of high-velocity magnetosheath populations (Figure 3b), pointing primarily along the $+Y-X$ direction, which is quasi-parallel to the shear flow direction (see the arrows in Figure 4a). The magnitude of the ion heat flux is basically steady across the trailing edge (approximately 0.5 mW/m^2), but its direction changes dramatically into the $-Y$ direction at the trailing edge (Figure 3e). The electron enthalpy flux (Figure 3g) and kinetic energy flux (Figure 3h) also increase across the trailing edge because of the increase in electron velocity (Figure 3f), but their magnitudes are insignificant compared with that of the ion energy flux. The electron heat flux is also negligible and remains steady (Figure 3i). The Poynting flux also increases significantly across the trailing edge because of the enhancement of electromagnetic fields and the change in its direction from $+Z-X$ to $+Y-X$, carrying a significant portion of energy flux densities

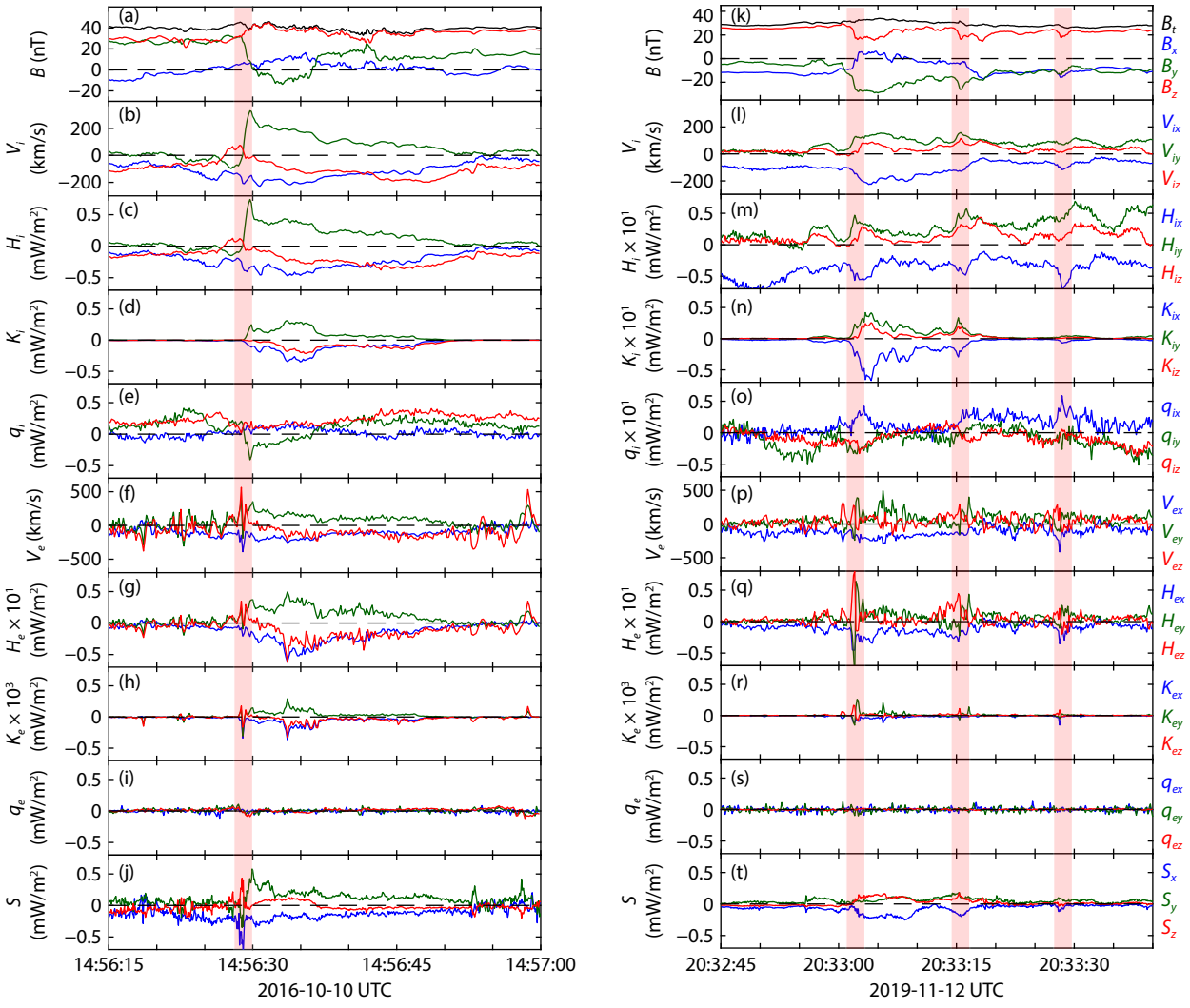

Figure 3. Energy flux densities at the linear KH vortex (left) and nonlinear KH vortex (right). (a, k) Magnetic field; (b, l) ion velocity; (c, m) ion enthalpy flux density; (d, n) ion kinetic energy flux density; (e, o) ion thermal flux density; (f, p) electron velocity; (g, q) electron enthalpy flux density; (h, r) electron kinetic energy flux density; (i, s) electron thermal flux density; (j, t) Poynting flux density. For easy comparison, the range of the Y-axis is set as a fixed value and the very small flux densities (e.g., electron kinetic energy flux) are plotted by multiplying a constant. The red shaded areas mark the trailing edge of the vortices.

(Figure 3j). Therefore, the ion energy flux and the Poynting flux are dominant in this case.

At the nonlinear KH vortex, the ion enthalpy flux (Figure 3m), kinetic energy flux (Figure 3n) and heat flux (Figure 3o) have maximum magnitude, reaching higher than 0.05 mW/m². Although the ion enthalpy flux and heat flux are generally large on both the magnetosphere side and the magnetosheath side, the ion kinetic energy flux is much larger on the magnetosheath side. However, all these fluxes are enhanced or reach their maximum magnitudes simultaneously at the multiple encounters of the rolled-up trailing edge (20:33:02, 20:33:16, and 20:33:28 UT). Note that the maximum magnitude of the electron enthalpy flux (Figure 3q) is even higher than that of the ion enthalpy flux (Figure 3m), which is also correlated with variation in the magnetic field. Similar to the linear KH vortex, the electron kinetic energy flux also shows an insignificant portion of local increases because of the small mass of the electron population (Figure 3r), and the electron heat flux is basically negligible (Figure 3s). Note that the enthalpy flux and the kinetic energy flux are mainly along the $-X+Y+Z$ direction, which also corresponds to the shear flow direction. The Poynting flux is also largely increased across the trailing edge of the KH vortex and is dominated by steady $+S_Y$ and $+S_Z$ components. As such, the energy flux density in this case is dominated by the Poynting flux, which is very structured and correlated to variation in the magnetic field at the boundary (see the magenta arrow in Figure 4b).

Note that the energy flux densities exhibit peaks at the trailing edge of the KH vortices, where the largest energy conversion rate is also observed (Figure 2). The energy flux densities on the magnetospheric side are generally smaller than those on the magnetosheath side, which is likely a natural consequence of the plasma density contrast between the magnetosphere and magnetosheath. To investigate whether the energy budgets at these two KH vortices share a similar constitution and to determine which types of energy fluxes dominate the energy transfer process, in Figure 4 we show the distributions of different energy flux densities as a function of the local energy conversion. The data points are from the same interval as in Figures 2 and 3. For the linear KH case, we find that the ion enthalpy, ion heat, and Poynting flux densities are generally higher than the ion kinetic and electron enthalpy densities (Figure 4c), suggesting that the energy transport at the linear KH vortex is mainly contributed by the ion energy flux and the Poynting flux, with negligible contribution by the electron

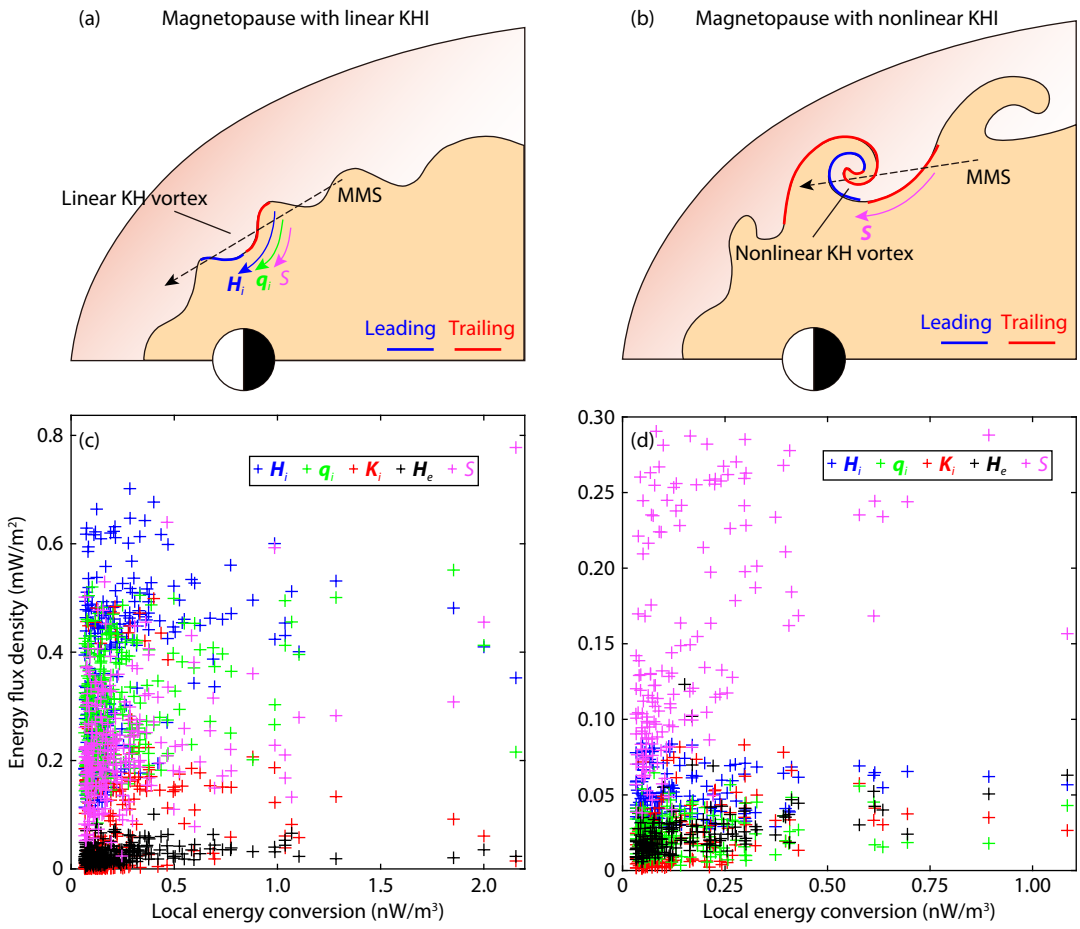

Figure 4. Sketch depicting the configuration of the magnetopause with the KHI and the characteristics of energy conversion and energy flux densities at the linear KH vortex (a, c) and nonlinear KH vortex (b, d). The blue, green, red, black, and magenta points represent the ion enthalpy flux, ion heat flux, ion kinetic flux, electron enthalpy flux, and Poynting flux, respectively. The dashed lines in (a) and (b) represent the MMS trajectory.

energy flux. For the nonlinear KH vortex, we find that the Poynting flux densities are much larger than the other forms of energy flux densities (Figure 4d), indicating that the energy there is transported mainly in the form of Poynting fluxes. Therefore, we conclude that energy transport can be very different at the linear KH vortex and the nonlinear KH vortex (Figures 4a and 4b).

3. Conclusion and Discussion

In this study, using MMS measurements, we present an *in situ* investigation of the characteristics of energy conversion and energy flux densities at a linear KH vortex and a nonlinear KH vortex. We find that the linear KH vortex is basically a generator region ($\boldsymbol{J}\cdot\boldsymbol{E} < 0$) where energy is transferred from the plasma to the magnetic field. At the trailing edge of the linear KH vortex, the ion enthalpy flux, Poynting flux, and ion heat flux increase drastically, collaboratively carry the greatest portion of energy, and correlate with the local energy conversion rate. In contrast, the nonlinear KH vortex is a load region ($\boldsymbol{J}\cdot\boldsymbol{E} > 0$) that converts electromagnetic energy into the kinetic and thermal energy of the plasma. Across the trailing edge of the nonlinear KH vortex, small-scale magnetic structures are formed because of the existence of secondary vortices. The Poynting flux increases quasi-linearly with local energy conversion and carries the greatest portion of energy. In both cases, the ion kinetic energy flux increases but contributes a relatively smaller portion; electron energy fluxes are basically negligible except that the electron enthalpy flux becomes comparable to the ion energy flux at the trailing edge of the nonlinear KH vortex. However, it should also be pointed out that these results cannot represent the general patterns of the KH vortex because this is a case study. To address this issue, further statistical investigations should be conducted.

The different properties of the energy flux intensities in the two cases may be related to the process of KH vortex development. At the linear stage, the KH vortex begins to form by the shear flow of the propagating linear surface wave, gradually deforming the magnetopause and gaining energy from the ions in the boundary layer. The fluid motion of the linear KH vortex can drive magnetic convection and turbulence (Hasegawa, 2012; Archer et al., 2024), which is probably why it acts as a generator region. As the KH vortex fully develops and eventually becomes the nonlinear roll-up vortex, the magnetic field lines are sufficiently twisted. The distortion and stretching of field lines can potentially lead to magnetic reconnection and can form magnetic islands (Hasegawa et al., 2009; Wang Z et al., 2022), which convert magnetic energy into kinetic and thermal energy (Nakamura et al., 2008; Wang RS et al., 2010, 2023; Huang SY et al., 2012b, 2019; Zhou M et al., 2017; Zhong ZH et al., 2018; Jiang K et al., 2021; Wang Z et al., 2023a, b). Moreover, plasma mixing is sufficiently increased at the nonlinear stage, which increases the turbulence and leads to diffusion (Zhang WZ et al., 2023). Therefore, the nonlinear KH vortex can act as a load region, and the electron enthalpy flux there can even be comparable to the ion energy flux.

Our study also emphasizes that the trailing edge of the KH vortex is an important location for energy conversion in the Earth's magnetosphere. In both cases, the magnitude of the energy conversion rate can reach approximately 1 nW/m^3, which is smaller than the super strong energy conversion (~2–6 nW/m^3) driven by the twisted magnetic structure at the Earth's magnetopause (Du CX et al., 2023) but similar to the energy conversion rate (approximately 1 nW/m^3) observed at the reconnection front (Huang SY et al., 2012b, 2015; Fu HS et al., 2013, 2017, 2019c; Du CX et al., 2024a; Jiang K et al., 2024, 2025) and the plasma sheet boundary layer (Du CX et al., 2024b). Considering that the spatial scale of the KH vortex is much larger than that of the aforementioned magnetic structures, the total amount of energy converted by the KH vortices should be very large. Therefore, the KH vortex can act as an important channel for transporting solar wind energy into the Earth's magnetosphere.

Acknowledgments

This work was supported by the National Natural Science Foundation of China (NSFC; Grant Nos. 42504163, 42241113, and 425B2026) and "the Fundamental Research Funds for the Central Universities." The authors thank the National Key R&D Program of China (Grant No. 2025YFF0512100) and the International Space Science Institute's (ISSI's) International Teams program (Grant No. 611 Kelvin–Helmholtz Instability Wave Investigation [KHIWI]) for support.

Open Research

The spacecraft data used for this study are from the MMS Science Data Center and are publicly available at https://lasp.colorado.edu/mms/sdc/public/about/browse-wrapper/.

References

Archer, M. O., Pilipenko, V. A., Li, B., Sorathia, K., Nakariakov, V. M., Elsden, T., and Nykyri, K. (2024). Magnetopause MHD surface wave theory: Progress & challenges. *Front. Astron. Space Sci.*, *11*, 1407172. https://doi.org/10.3389/fspas.2024.1407172

Burch, J. L., Torbert, R. B., Phan, T. D., Chen, L. J., Moore, T. E., Ergun, R. E., Eastwood, J. P., Gershman, D. J., Cassak, P. A., … Chandler, M. (2016a). Electron-scale measurements of magnetic reconnection in space. *Science*, *352*(6290), aaf2939. https://doi.org/10.1126/science.aaf2939

Burch, J. L., Moore, T. E., Torbert, R. B., and Giles, B. L. (2016b). Magnetospheric multiscale overview and science objectives. *Space Sci. Rev.*, *199*(1–4), 5–21. https://doi.org/10.1007/s11214-015-0164-9

Cao, D., Fu, H. S., Cao, J. B., Wang, T. Y., Graham, D. B., Chen, Z. Z., Peng, F. Z., Huang, S. Y., Khotyaintsev, Y. V., … Burch, J. L. (2017). MMS observations of whistler waves in electron diffusion region. *Geophys. Res. Lett.*, *44*(9), 3954–3962. https://doi.org/10.1002/2017GL072703

Cassak, P. A., Genestreti, K. J., Burch, J. L., Phan, T. D., Shay, M. A., Swisdak, M., Drake, J. F., Price, L., Eriksson, S., … Komar, C. M. (2017). The effect of a guide field on local energy conversion during asymmetric magnetic reconnection: Particle-in-cell simulations. *J. Geophys. Res.: Space Phys.*, *122*(11), 11523–11542. https://doi.org/10.1002/2017JA024555

Chandrasekhar, S. (1961). *Hydrodynamic and Hydromagnetic Stability*. Oxford: Clarendon Press.

Chang, C., Huang, K., Lu, S., Wang, R. S., and Lu, Q. M. (2023). Energy conversion during asymmetric magnetic reconnection. *Astrophys. J.*, *943*(2), 73. https://doi.org/10.3847/1538-4357/acaa3d

Chen, L. J., Hesse, M., Wang, S., Gershman, D., Ergun, R., Pollock, C., Torbert, R., Bessho, N., Daughton, W., … Avanov, L. (2016). Electron energization and mixing observed by MMS in the vicinity of an electron diffusion region during magnetopause reconnection. *Geophys. Res. Lett.*, *43*(12), 6036–6043.

https://doi.org/10.1002/2016GL069215

Cowee, M. M., Winske, D., and Gary, S. P. (2009). Two-dimensional hybrid simulations of superdiffusion at the magnetopause driven by Kelvin-Helmholtz instability. *J. Geophys. Res.: Space Phys.*, *114*(A10), A10209. https://doi.org/10.1029/2009JA014222

De Keyser, J., Dunlop, M. W., Owen, C. J., Sonnerup, B. U. Ö., Haaland, S. E., Vaivads, A., Paschmann, G., Lundin, R., and Rezeau, L. (2005). Magnetopause and boundary layer. *Space Sci. Rev.*, *118*(1–4), 231–320. https://doi.org/10.1007/s11214-005-3834-1

Dong, X. C., Dunlop, M. W., Wang, T. Y., Cao, J. B., Trattner, K. J., Bamford, R., Russell, C. T., Bingham, R., Strangeway, R. J., … Torbert, R. B. (2018). Carriers and sources of magnetopause current: MMS case study. *J. Geophys. Res.: Space Phys.*, *123*(7), 5464–5475. https://doi.org/10.1029/2018JA025292

Dong, X. C., Dunlop, M. W., Wang, T. Y., Zhao, J. S., Fu, H. S., Chen, Z. Z., Russell, C. T., Giles, B., Ergun, R., and Lindqvist, P. (2021). Observation of nonuniform energy dissipation in the electron diffusion region of magnetopause reconnection. *Geophys. Res. Lett.*, *48*(13), e2020GL091928. https://doi.org/10.1029/2020GL091928

Du, C. X., Fu, H. S., Wang, Z., Cao, J. B., Liu, Y. Y., and Fu, W. D. (2023). Energy conversion by a twisted magnetic structure at magnetopause boundary layer: MMS observations. *Geophys. Res. Lett.*, *50*(24), e2023GL106941. https://doi.org/10.1029/2023GL106941

Du, C. X., Wang, Z., Fu, H. S., Fu, W. D., Cao, J. B., Grigorenko, E., and Yu, Y. (2024a). Strong field-aligned current and its driven energy conversion at anti-dipolarization front. *Geophys. Res. Lett.*, *51*(16), e2024GL110017. https://doi.org/10.1029/2024GL110017

Du, C. X., Fu, H. S., Cao, J. B., Wang, Z., Yu, Y., Fu, W. D., and Zhang, W. Z. (2024b). Strong energy conversion at magnetotail plasma sheet boundary layer. *Geophys. Res. Lett.*, *51*(18), e2024GL111284. https://doi.org/10.1029/2024GL111284

Dunlop, M. W., A. Balogh, K.-H. Glassmeier, and P. Robert. (2002). Four-point Cluster application of magnetic field analysis tools: The Curlometer. *J. Geophys. Res.*, *107*(A11), 1384 https://doi.org/10.1029/2001JA005088

Dunlop, M. W., and Balogh, A. (2005). Magnetopause current as seen by Cluster. *Ann. Geophys.*, *23*(3), 901–907. https://doi.org/10.5194/angeo-23-901-2005

Eastman, T. E., Boardsen, S. A., Chen, S. H., Fung, S. F., and Kessel, R. L. (2000). Configuration of high-latitude and high-altitude boundary layers. *J. Geophys. Res.: Space Phys.*, *105*(A10), 23221–23238. https://doi.org/10.1029/1999JA900269

Eastwood, J. P., Phan, T. D., Drake, J. F., Shay, M. A., Borg, A. L., Lavraud, B., and Taylor, M. G. G. T. (2013). Energy partition in magnetic reconnection in Earth's magnetotail. *Phys. Rev. Lett.*, *110*(22), 225001. https://doi.org/10.1103/PhysRevLett.110.225001

Eastwood, J. P., Goldman, M. V., Phan, T. D., Stawarz, J. E., Cassak, P. A., Drake, J. F., Newman, D., Lavraud, B., Shay, M., … Tussell, C. T. (2020). Energy flux densities near the electron dissipation region in asymmetric magnetopause reconnection. *Phys. Rev. Lett.*, *125*(26), 265102. https://doi.org/10.1103/PhysRevLett.125.265102

Ergun, R. E., Tucker, S., Westfall, J., Goodrich, K. A., Malaspina, D. M., Summers, D., Wallace, J., Karlsson, M., Mack, J., … Cully, C. M. (2016). The axial double probe and fields signal processing for the MMS mission. *Space Sci. Rev.*, *199*(1), 167–188. https://doi.org/10.1007/s11214-014-0115-x

Fairfield, D. H., Otto, A., Mukai, T., Kokubun, S., Lepping, R. P., Steinberg, J. T., Lazarus, A. J., and Yamamoto, T. (2000). Geotail observations of the Kelvin-Helmholtz instability at the equatorial magnetotail boundary for parallel northward fields. *J. Geophys. Res.: Space Phys.*, *105*(A9), 21159–21173. https://doi.org/10.1029/1999JA000316

Fargette, N., Eastwood, J. P., Waters, C. L., Øieroset, M., Phan, T. D., Newman, D. L., Stawarz, J. E., Goldman, M. V., and Lapenta, G. (2024). Statistical study of energy transport and conversion in electron diffusion regions at Earth's dayside magnetopause. *J. Geophys. Res.: Space Phys.*, *129*(10), e2024JA032897. https://doi.org/10.1029/2024JA032897

Foullon, C., Farrugia, C. J., Fazakerley, A. N., Owen, C. J., Gratton, F. T., and Torbert, R. B. (2008). Evolution of Kelvin-Helmholtz activity on the dusk flank magnetopause. *J. Geophys. Res.: Space Phys.*, *113*(A11), A11203. https://doi.org/10.1029/2008JA013175

Fu, H. S., Khotyaintsev, Y. V., Vaivads, A., Retinò, A., and André, M. (2013). Energetic electron acceleration by unsteady magnetic reconnection. *Nat. Phys.*, *9*(7), 426–430. https://doi.org/10.1038/NPHYS2664

Fu, H. S., Vaivads, A., Khotyaintsev, Y. V., André, M., Cao, J. B., Olshevsky, V., Eastwood, J. P., and Retinò, A. (2017). Intermittent energy dissipation by turbulent reconnection. *Geophys. Res. Lett.*, *44*(1), 37–43. https://doi.org/10.1002/2016GL071787

Fu, H. S., Peng, F. Z., Liu, C. M., Burch, J. L., Gershman, D. G., and Le Contel, O. (2019a). Evidence of electron acceleration at a reconnecting magnetopause. *Geophys. Res. Lett.*, *46*(11), 5645–5652. https://doi.org/10.1029/2019GL083032

Fu, H. S., Cao, J. B., Cao, D., Wang, Z., Vaivads, A., Khotyaintsev, Y. V., Burch, J. L., and Huang, S. Y. (2019b). Evidence of magnetic nulls in electron diffusion region. *Geophys. Res. Lett.*, *46*(1), 48–54. https://doi.org/10.1029/2018GL080449

Fu, H. S., Xu, Y., Vaivads, A., and Khotyaintsev, Y. V. (2019c). Super-efficient electron acceleration by an isolated magnetic reconnection. *Astrophys. J. Lett.*, *870*(2), L22. https://doi.org/10.3847/2041-8213/aafa75

Fu, W. D., Fu, H. S., Zhang, W. Z., Yu, Y., and Cao, J. B. (2025a). Compression of Earth's magnetopause down to 5 R_E during the superstorm on 10 May 2024. *Geophys. Res. Lett.*, *52*(5), e2024GL114040. https://doi.org/10.1029/2024GL114040

Fu, W. D., Fu, H. S., Wang, C., Dai, L., Han, D. S., Yu, Y., Wang, Z., Toledo-Redondo, S., Hwang, K. J., and Nakamura, R. (2025b). On the dipolarization front and magnetopause: 3. Evidence of electron Kelvin–Helmholtz instability at dipolarization front. *J. Geophys. Res.: Space Phys.*, *130*(8), e2025JA034096. https://doi.org/10.1029/2025JA034096

Genestreti, K. J., Li, X. C., Liu, Y. H., Burch, J. L., Torbert, R. B., Fuselier, S. A., Nakamura, T., Giles, B. L., Gershman, D. J., … Strangeway, R. J. (2022). On the origin of "patchy" energy conversion in electron diffusion regions. *Phys. Plasmas*, *29*(8), 082107. https://doi.org/10.1063/5.0090275

Goldman, M. V., Newman, D. L., and Lapenta, G. (2016). What can we learn about magnetotail reconnection from 2D PIC Harris-sheet simulations?. *Space Sci. Rev.*, *199*(1-4), 651–688. https://doi.org/10.1007/s11214-015-0154-y

Hasegawa, H., Fujimoto, M., Takagi, K., Saito, Y., Mukai, T., and Rème, H. (2006). Single-spacecraft detection of rolled-up Kelvin-Helmholtz vortices at the flank magnetopause. *J. Geophys. Res.: Space Phys.*, *111*(A9), A09203. https://doi.org/10.1029/2006JA011728

Hasegawa, H., Retinò, A., Vaivads, A., Khotyaintsev, Y., André, M., Nakamura, T. K. M., Teh, W. L., Sonnerup, B. U. Ö., Schwartz, S. J., … Canu, P. (2009). Kelvin-Helmholtz waves at the Earth's magnetopause: Multiscale development and associated reconnection. *J. Geophys. Res.: Space Phys.*, *114*(A12), A12207. https://doi.org/10.1029/2009JA014042

Hasegawa, H. (2012). Structure and dynamics of the magnetopause and its boundary layers. *Monogr. Environ. Earth Planets*, *1*(2), 71–119. https://doi.org/10.5047/meep.2012.00102.0071

Huang, S. Y., Vaivads, A., Khotyaintsev, Y. V., Zhou, M., Fu, H. S., Retinò, A., Deng, X. H., André, M., Cully, C. M., … Pang, Y. (2012a). Electron acceleration in the reconnection diffusion region: Cluster observations. *Geophys. Res. Lett.*, *39*(11), L11103. https://doi.org/10.1029/2012GL051946

Huang, S. Y., Zhou, M., Deng, X. H., Yuan, Z. G., Pang, Y., Wei, Q., Su, W., Li, H. M., and Wang, Q. Q. (2012b). Kinetic structure and wave properties associated with sharp dipolarization front observed by Cluster. *Ann. Geophys.*, *30*(1), 97–107. https://doi.org/10.5194/angeo-30-97-2012

Huang, S. Y., Fu, H. S., Yuan, Z. G., Zhou, M., Fu, S., Deng, X. H., Sun, W. J., Pang, Y., Wang, D. D., … Yu, X. D. (2015). Electromagnetic energy conversion at dipolarization fronts: Multispacecraft results. *J. Geophys. Res.: Space Phys.*, *120*(6), 4496–4502. https://doi.org/10.1002/2015JA021083

Huang, S. Y., Jiang, K., Yuan, Z. G., Zhou, M., Sahraoui, F., Fu, H. S., Deng, X. H., Khotyaintsev, Y. V., Yu, X. D., … Burch, J. L. (2019). Observations of flux ropes with strong energy dissipation in the magnetotail. *Geophys. Res. Lett.*, *46*(2), 580–589. https://doi.org/10.1029/2018GL081099

Huang, S. Y., Xiong, Q. Y., Song, L. F., Nan, J., Yuan, Z. G., Jiang, K., Deng, X. H.,

and Yu, L. (2021). Electron-only reconnection in an ion-scale current sheet at the magnetopause. *Astrophys. J.*, *922*(1), 54. https://doi.org/10.3847/1538-4357/ac2668

Huang, S. Y., Xiong, Q. Y., Jiang, K., Yuan, Z. G., Lin, R. T., and Tang, Y. T. (2025). Recent advances on kinetic simulations and observations of electron diffusion region during magnetic reconnection in space plasmas. *Rev. Mod. Plasma Phys.*, *9*(1), 4. https://doi.org/10.1007/s41614-025-00179-6

Hwang, K. J., Goldstein, M. L., Kuznetsova, M. M., Wang, Y., Viñas, A. F., and Sibeck, D. G. (2012). The first in situ observation of Kelvin-Helmholtz waves at high-latitude magnetopause during strongly dawnward interplanetary magnetic field conditions. *J. Geophys. Res.: Space Phys.*, *117*(A8), A08233. https://doi.org/10.1029/2011JA017256

Jiang, K., Huang, S. Y., Yuan, Z. G., Deng, X. H., Wei, Y. Y., Xiong, Q. Y., Xu, S. B., Zhang, J., Zhang, Z. H., … Yu, L. (2021). Statistical properties of current, energy conversion, and electron acceleration in flux ropes in the terrestrial magnetotail. *Geophys. Res. Lett.*, *48*(11), e2021GL093458. https://doi.org/10.1029/2021GL093458

Jiang, K., Huang, S. Y., Yuan, Z. G., Xiong, Q. Y., Xu, S. B., and Lin, R. T. (2024). Observations of energy conversion caused by magnetic reconnection at a dipolarization front. *Geophys. Res. Lett.*, *51*(6), e2023GL107919. https://doi.org/10.1029/2023GL107919

Jiang, K., Huang, S. Y., Lu, Q. M., Yuan, Z. G., and Xiong, Q. Y. (2025). Observations of the electromagnetic electron Kelvin–Helmholtz instability and its impact on the dynamics inside a flux rope. *Geophys. Res. Lett.*, *52*(1), e2024GL111450. https://doi.org/10.1029/2024GL111450

Johnson, J. R., and Cheng, C. Z. (1997). Kinetic Alfvén waves and plasma transport at the magnetopause. *Geophys. Res. Lett.*, *24*(11), 1423–1426. https://doi.org/10.1029/97GL01333

Kavosi, S., and Raeder, J. (2015). Ubiquity of Kelvin–Helmholtz waves at Earth's magnetopause. *Nat. Commun.*, *6*(1), 7019. https://doi.org/10.1038/ncomms8019

Le, G., and Russell, C. T. (1994). The thickness and structure of high beta magnetopause current layer. *Geophys. Res. Lett.*, *21*(23), 2451–2454. https://doi.org/10.1029/94GL02292

Li, W., André, M., Khotyaintsev, Y. V., Vaivads, A., Graham, D. B., Toledo-Redondo, S., Norgren, C., Henri, P., Wang, C., … Strangeway, R. J. (2016). Kinetic evidence of magnetic reconnection due to Kelvin-Helmholtz waves. *Geophys. Res. Lett.*, *43*(11), 5635–5643. https://doi.org/10.1002/2016GL069192

Liu, Y. N., Fujimoto, K., Wang, J. Q., and Duan, X. C. (2024). Energy conversion due to non-ideal electric field in separatrix region of magnetotail reconnection. *Earth Planet. Phys.*, *8*(5), 787–796. https://doi.org/10.26464/epp2024055

Lin, D., Wang, C., Li, W. Y., Tang, B. B., Guo, X. C., and Peng, Z. (2014). Properties of Kelvin-Helmholtz waves at the magnetopause under northward interplanetary magnetic field: Statistical study. *J. Geophys. Res.: Space Phys.*, *119*(9), 7485–7494. https://doi.org/10.1002/2014JA020379

Lin, R. L., Zhang, X. X., Liu, S. Q., Wang, Y. L., and Gong, J. C. (2010). A three-dimensional asymmetric magnetopause model. *J. Geophys. Res.: Space Phys.*, *115*(A4), A04207. https://doi.org/10.1029/2009JA014235

Lindqvist, P. A., Olsson, G., Torbert, R. B., King, B., Granoff, M., Rau, D., Needell, G., Turco, S., Dors, I., … Tucker, S. (2016). The spin-plane double probe electric field instrument for MMS. *Space Sci. Rev.*, *199*(1), 137–165. https://doi.org/10.1007/s11214-014-0116-9

Miura, A. (1984). Anomalous transport by magnetohydrodynamic Kelvin-Helmholtz instabilities in the solar wind-magnetosphere interaction. *J. Geophys. Res.: Space Phys.*, *89*(A2), 801–818. https://doi.org/10.1029/JA089iA02p00801

Nakamura, T. K. M., Fujimoto, M., and Otto, A. (2008). Structure of an MHD-scale Kelvin-Helmholtz vortex: Two-dimensional two-fluid simulations including finite electron inertial effects. *J. Geophys. Res.: Space Phys.*, *113*(A9), A09204. https://doi.org/10.1029/2007JA012803

Nakamura, T. K. M., Blasl, K. A., Liu, Y. H., and Peery, S. A. (2022). Diffusive plasma transport by the magnetopause Kelvin-Helmholtz instability during southward IMF. *Front. Astron. Space Sci.*, *8*, 809045. https://doi.org/10.3389/fspas.2021.809045

Nykyri, K., and Otto, A. (2001). Plasma transport at the magnetospheric boundary due to reconnection in Kelvin-Helmholtz vortices. *Geophys. Res. Lett.*, *28*(18), 3565–3568. https://doi.org/10.1029/2001GL013239

Nykyri, K., Ma, X. Y., Dimmock, A., Foullon, C., Otto, A., and Osmane, A. (2017). Influence of velocity fluctuations on the Kelvin-Helmholtz instability and its associated mass transport. *J. Geophys. Res.: Space. Phys.*, *122*(9), 9489–9512. https://doi.org/10.1002/2017JA024374

Otto, A., and Fairfield, D. H. (2000). Kelvin-Helmholtz instability at the magnetotail boundary: MHD simulation and comparison with geotail observations. *J. Geophys. Res.: Space Phys.*, *105*(A9), 21175–21190. https://doi.org/10.1029/1999JA000312

Palmroth, M., Pulkkinen, T. I., Janhunen, P., and Wu, C. C. (2003). Stormtime energy transfer in global MHD simulation. *J. Geophys. Res.: Space Phys.*, *108*(A1), 1048. https://doi.org/10.1029/2002JA009446

Palmroth, M., Laitinen, T. V., and Pulkkinen, T. I. (2006). Magnetopause energy and mass transfer: Results from a global MHD simulation. *Ann. Geophys.*, *24*(12), 3467–3480. https://doi.org/10.5194/angeo-24-3467-2006

Phan, T. D., Larson, D., McFadden, J., Lin, R. P., Carlson, C., Moyer, M., Paularena, K. I., McCarthy, M., Parks, G. K., … Lepping, R. P. (1997). Low-latitude dusk flank magnetosheath, magnetopause, and boundary layer for low magnetic shear: Wind observations. *J. Geophys. Res.: Space Phys.*, *102*(A9), 19883–19895. https://doi.org/10.1029/97JA01596

Pollock, C., Moore, T., Jacques, A., Burch, J., Gliese, U., Saito, Y., Omoto, T., Avanov, L., Barrie, A., … Zeuch, M. (2016). Fast plasma investigation for magnetospheric multiscale. *Space Sci. Rev.*, *199*(1–4), 331–406. https://doi.org/10.1007/s11214-016-0245-4

Pu, Z. Y., and Kivelson, M. G. (1983). Kelvin-Helmholtz instability at the magnetopause: Energy flux into the magnetosphere. *J. Geophys. Res.*, *88*(A2), 853–861. https://doi.org/10.1029/ja088ia02p00853

Radhakrishnan, D. K. V., Fuselier, S. A., Petrinec, S. M., Rice, R. C., Nykyri, K., Trattner, K. J., Gershman, D. J., and Burch, J. L. (2024). Evidence of plasma mixing at the Earth's magnetopause due to Kelvin Helmholtz vortices. *J. Geophys. Res.: Space Phys.*, *129*(9), e2024JA032869. https://doi.org/10.1029/2024JA032869

Rice, R. C., Nykyri, K., Ma, X. Y., and Burkholder, B. L. (2022). Characteristics of Kelvin–Helmholtz waves as observed by the MMS from September 2015 to March 2020. *J. Geophys. Res.: Space Phys.*, *127*(3), e2021JA029685. https://doi.org/10.1029/2021JA029685

Russell, C. T., Anderson, B. J., Baumjohann, W., Bromund, K. R., Dearborn, D., Fischer, D., Le, G., Leinweber, H. K., Leneman, D., … Richter, I. (2016). The magnetospheric multiscale magnetometers. *Space Sci. Rev.*, *199*(1–4), 189–256. https://doi.org/10.1007/s11214-014-0057-3

Settino, A., Khotyaintsev, Y. V., Graham, D. B., Perrone, D., and Valentini, F. (2022). Characterizing satellite path through Kelvin-Helmholtz instability using a mixing parameter. *J. Geophys. Res.: Space Phys.*, *127*(2), e2021JA029758. https://doi.org/10.1029/2021JA029758

Shue, J. H., Song, P., Russell, C. T., Steinberg, J. T., Chao, J. K., Zastenker, G., Vaisberg, O. L., Kokubun, S., Singer, H. J., … Kawano, H. (1998). Magnetopause location under extreme solar wind conditions. *J. Geophys. Res.: Space Phys.*, *103*(A8), 17691–17700. https://doi.org/10.1029/98JA01103

Smets, R., Delcourt, D., Chanteur, G., and Moore, T. E. (2002). On the incidence of Kelvin-Helmholtz instability for mass exchange process at the Earth's magnetopause. *Ann. Geophys.*, *20*(6), 757–769. https://doi.org/10.5194/angeo-20-757-2002

Sorathia, K. A., Merkin, V. G., Ukhorskiy, A. Y., Allen, R. C., Nykyri, K., and Wing, S. (2019). Solar wind ion entry into the magnetosphere during northward IMF. *J. Geophys. Res.: Space Phys.*, *124*(7), 5461–5481. https://doi.org/10.1029/2019JA026728

Sun, T. R., Connor, H., and Samsonov, A. (2024). Preface to the Special Issue on Modeling and Data Analysis Methods for the SMILE mission. *Earth Planet. Phys.*, *8*(1), 1–4. https://doi.org/10.26464/epp2023089

Wang, R. S., Lu, Q. M., Du, A. M., and Wang, S. (2010). *In situ* observations of a secondary magnetic island in an ion diffusion region and associated energetic electrons. *Phys. Rev. Lett.*, *104*(17), 175003. https://doi.org/10.1103

/PhysRevLett.104.175003

Wang, R. S., Wang, S. M., Lu, Q. M., Li, X. M., Lu, S., and Gonzalez, W. (2023). Direct observation of turbulent magnetic reconnection in the solar wind. *Nat. Astron.*, *7*(1), 18–28. https://doi.org/10.1038/s41550-022-01818-5

Wang, Z., Fu, H. S., Liu, C. M., Liu, Y. Y., Cozzani, G., Giles, B. L., Hwang, K. J., and Burch, J. L. (2019). Electron distribution functions around a reconnection X-line resolved by the FOTE method. *Geophys. Res. Lett.*, *46*(3), 1195–1204. https://doi.org/10.1029/2018GL081708

Wang, Z., Fu, H. S., Vaivads, A., Burch, J. L., Yu, Y., and Cao, J. B. (2020a). Monitoring the spatio-temporal evolution of a reconnection X-line in space. *Astrophys. J. Lett.*, *899*(2), L34. https://doi.org/10.3847/2041-8213/abad2c

Wang, Z., Fu, H. S., Olshevsky, V., Liu, Y. Y., Liu, C. M., and Chen, Z. Z. (2020b). Extending the FOTE method to three-dimensional plasma flow fields. *Astrophys. J. Suppl. Ser.*, *249*(1), 10. https://doi.org/10.3847/1538-4365/ab95a0

Wang, Z., Fu, H. S., Chen, X. H., Cao, J. B., Liu, Y. Y., Yu, Y., He, R. J., and Guo, Z. Z. (2022). The effect of current on magnetic null topology during turbulent reconnection. *Astrophys. J.*, *927*(1), 119. https://doi.org/10.3847/1538-4357/ac4eed

Wang, Z., Vaivads, A., Fu, H. S., Cao, J. B., Lindberg, M., Turner, D. L., Ergun, R. E., and Liu, Y. Y. (2023a). Two-step acceleration of energetic electrons at magnetic flux ropes during turbulent reconnection. *Astrophys. J.*, *946*(2), 67. https://doi.org/10.3847/1538-4357/acc026

Wang, Z., Vaivads, A., Fu, H. S., Cao, J. B., and Liu, Y. Y. (2023b). Efficient electron acceleration driven by flux rope evolution during turbulent reconnection. *Astrophys. J.*, *946*(1), 39. https://doi.org/10.3847/1538-4357/acbd3e

Yao, Z. H., Guo, R. L., Wei, Y., Bonfond, B., Grodent, D., Zhang, B. Z., Dunn, W. R., and Pu, Z. Y. (2024). Recent advances in the magnetic reconnection, dipolarization, and auroral processes at giant planets from the perspective of comparative planetology. *Earth Planet. Phys.*, *8*(5), 659–672. https://doi.org/10.26464/epp2024017

Yamada, M., Kulsrud, R., and Ji, H. T. (2010). Magnetic reconnection. *Rev. Mod. Phys.*, *82*(1), 603–664. https://doi.org/10.1103/RevModPhys.82.603

Yan, G. Q., Parks, G. K., Cai, C. L., Chen, T., McFadden, J. P., and Ren, Y. (2020). Plasma transport into the duskside magnetopause caused by Kelvin–Helmholtz vortices in response to the northward turning of the interplanetary magnetic field observed by THEMIS. *Ann. Geophys.*, *38*(1), 263–273. https://doi.org/10.5194/angeo-38-263-2020

Zhang, W. Z., Fu, H. S., Cao, J. B., Wang, Z., and Liu, Y. Y. (2023). Properties of the turbulence and topology in a turbulent magnetic reconnection. *Astrophys. J.*, *953*(1), 23. https://doi.org/10.3847/1538-4357/acdacf

Zhong, Z. H., Tang, R. X., Zhou, M., Deng, X. H., Pang, Y., Paterson, W. R., Giles, B. L., Burch, J. L., Tobert, R. B., …Lindquist, P. A. (2018). Evidence for secondary flux rope generated by the electron Kelvin-Helmholtz instability in a magnetic reconnection diffusion region. *Phys. Rev. Lett.*, *120*(7), 075101. https://doi.org/10.1103/PhysRevLett.120.075101

Zhou, M., Berchem, J., Walker, R. J., El-Alaoui, M., Deng, X., Cazzola, E., Lapenta, G., Goldstein, M. L., Paterson, W. R., … Burch, J. L. (2017). Coalescence of macroscopic flux ropes at the subsolar magnetopause: Magnetospheric Multiscale observations. *Phys. Rev. Lett.*, *119*(5), 055101. https://doi.org/10.1103/PhysRevLett.119.055101